Electronic Supplementary Material (ESI) for ChemComm.

Supporting Information

of

A neutral *vicinal* silylene/phosphane supported unprecedented six-membered C_2PSiAu_2 ring and a silver(I) complex

Mohd Nazish,[a] Han Bai,[b] Christina M. Legendre,[a] Regine Herbst-Irmer,[a] Lili Zhao,*[b] Dietmar Stalke,*[a] and Herbert W. Roesky*[a]

Contents: **Page No.**

Experimental Section

Materials and Methods

Syntheses were carried out under an inert atmosphere of dinitrogen in oven- dried glassware using standard Schlenk techniques. All other manipulations were accomplished in a dinitrogen-filled glove box. Solvents were purified by MBRAUN solvent purification system MB SPS-800. All chemicals were purchased from Aldrich and used without further purification. $C_6H_4LSiPPh_2$ and $C_6H_4LSiAlCl_3PPh_2$ were prepared as reported in the literature. ^{1}H, ^{13}C, and ^{29}Si NMR spectra were recorded with a Bruker Avance DRX 500 spectrometer, using C_6D_6 as a solvent. Chemical shifts δ are given relative to $SiMe_4$. EI–MS spectra were obtained using a Finnigan MAT 8230 spectrometer. Elemental analyses were performed at the Institut für Anorganische Chemie, Universität Göttingen. For elemental analysis compounds were stored under vacuum for six hours to remove the solvent molecules. Melting points were measured in a sealed glass tube on a Büchi B-540 melting point apparatus.

Synthesis

$[C_6H_4(Ph(N^tBu)_2Si\text{-}Au(Cl)\text{--}Au(Cl)\text{-}P(Ph_2)]$ (2): A mixture of ligand **1** ($C_6H_4LSiPPh_2$) (0.52 g, 0.10 mmol) and $AuCl(SMe_2)$ (0.060 g, 0.20 mmol) was placed in 100 mL round bottom flask. Dichloromethane (30 mL) was added at room temperature and the reaction mixture was allowed to stir for 20 hr at the same temperature. The solution was filtered and concentrated to 10 mL under low vacuum. The filtered solution was stored at -30 °C in the freezer. After two months the colorless block-shaped X-ray quality crystals of **2** obtained from the concentrated solution of dichloromethane. Yield 0.075 mmol, 76%. MP: 245-250 °C. ^{1}H NMR (500 MHz, CD_2Cl_2, 298 K, ppm): δ 1.04 (s, 18 H, C*Me*$_3$), 7.30–7.40 (m, 12 H, Ar*H*), 7.53–7.73 (m, 7 H, Ar*H*). ^{13}C NMR (126 MHz, CD_2Cl_2, 298 K, ppm): δ 31.00, 54.24, 128.08, 128.98, 129.00, 130.48, 130.68, 130.85, 134.09, 134.19, 134.29, 134.55, 134.88, 195.16. ^{31}P NMR (160 MHz, CD_2Cl_2, 298 K, ppm): δ 25.57. ^{29}Si NMR (99 MHz, CD_2Cl_2, 298 K, ppm): δ 1.97 (d, $J_{Si\text{-}P}$ = 45.5 Hz). Elemental analysis (%) calcd. for $C_{33}H_{37}Au_2Cl_2N_2PSi$ (984.12): C, 40.22; H, 3.78; N, 2.84. Found: C, 40.62; H, 4.08; N, 3.17. MS (LIFDI, toluene): m/z = 984.09 ($[M+K]^+$).

$[C_6H_4LSiF_2PPh_2\text{-}Ag\text{-}PPh_2C_6H_4LSiF_2]^+[AlCl_4]^-$ (4): At 0 °C dichloromethane (30 mL) was added to a mixture of $AgSbF_6$ (0.026 g, 0.10 mmol) and $C_6H_4LSiPPh_2\text{-}AlCl_3$ (0.0280 g, 0.20 mmol). The reaction mixture was allowed to stir over night at room temperature. The solution was filtered and concentrated to 10 mL under low vacuum. The filtered solution was stored at 0 °C in the freezer. After one month the colorless block-shaped X-ray quality crystals of **4** obtained from the concentrated solution of dichloromethane. Yield 0.083 mmol, 60%. MP: 248-255 °C. ^{1}H NMR (500 MHz, CD_2Cl_2, 298 K, ppm): δ 0.79 (s, 36 H, C*Me*$_3$), 7.21–7.22 (m, 2 H, Ar*H*), 7.36–7.39 (m, 9 H, Ar*H*), 7.43–7.59 (m, 25 H, Ar*H*), 7.92–7.94 (m, 2 H, Ar*H*). ^{13}C NMR (126 MHz, CD_2Cl_2, 298 K, ppm): δ 31.23, 128.03, 128.34, 128.57, 128.84, 129.23, 129.26, 129.88, 130.26, 130.74, 130.95, 132.04, 134.48, 135.08, 176.31. ^{31}P NMR (160 MHz, CD_2Cl_2, 298 K, ppm): δ 9.12 (sextet, $J_{P\text{-}C}$ =25 Hz), 11.93 (sextet, $J_{P\text{-}C}$ =25 Hz). ^{29}Si NMR (99

MHz, CD_2Cl_2, 298 K, ppm): δ –97.77 (triplet, J_{Si-F} =255 Hz). ^{19}F NMR (25 MHz, CD_2Cl_2, 298 K, ppm): δ –107.98 (quartet, J_{Si-F} =150 Hz). Elemental analysis (%) calcd. for $C_{66}H_{74}AgAlCl_4F_4N_4P_2Si_2$ (1390.25): C, 56.86; H, 5.35; N, 4.02. Found: C, 56.68; H, 5.57; N, 4.71. MS (LIFDI, toluene): m/z = 1176.4 ($[M-AlCl_4-3F+Li+3H]^+$).

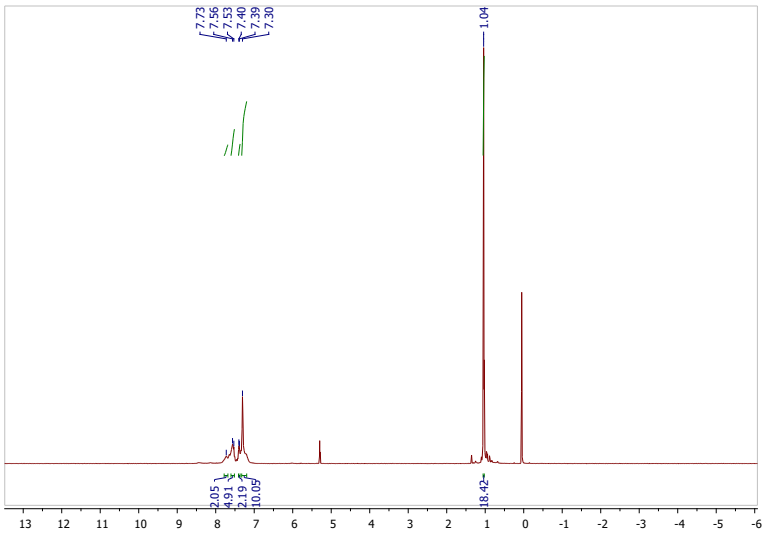

Figure S1: ^{1}H NMR spectrum of **2** at 298 K.

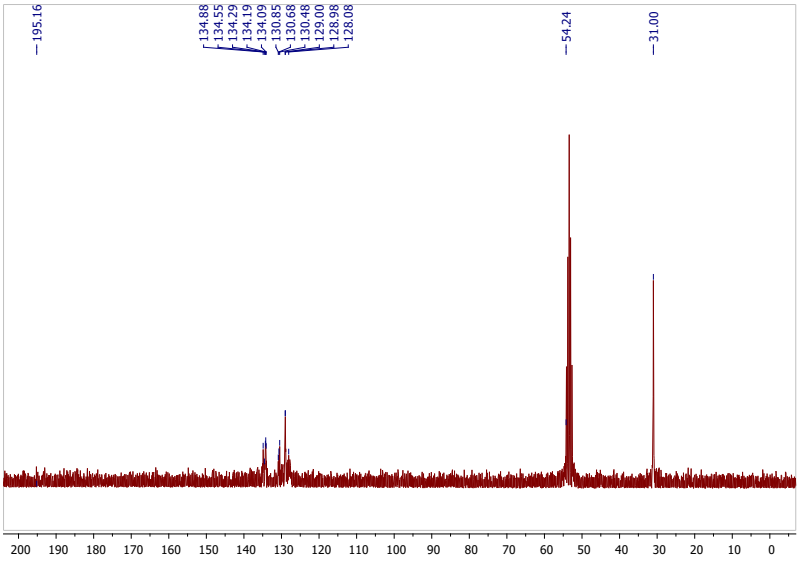

Figure S2: ^{13}C NMR spectrum of **2** at 298 K.

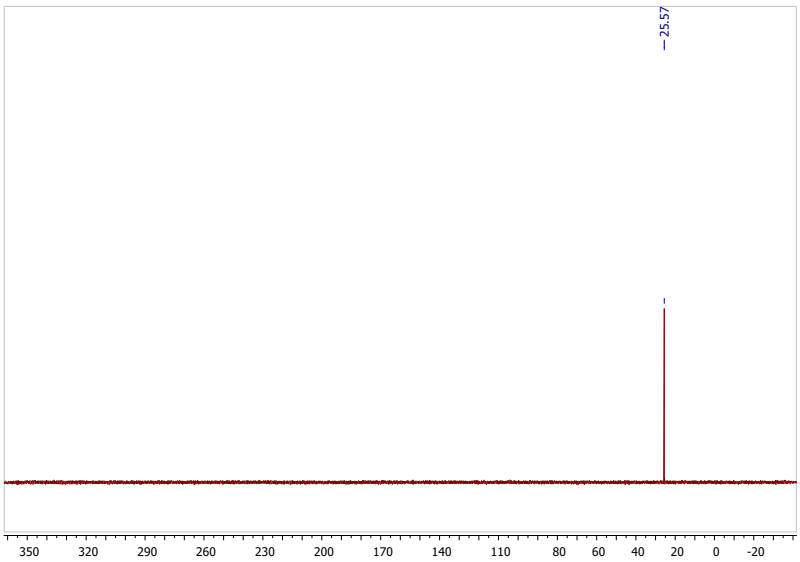

Figure S3: ^{31}P NMR spectrum of **2** at 298 K.

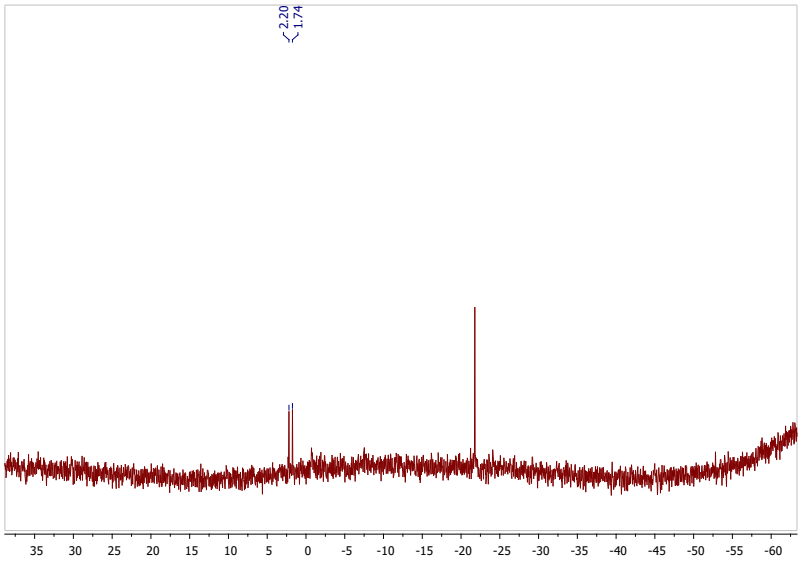

Figure S4: ^{31}Si NMR spectrum of **2** at 298 K.

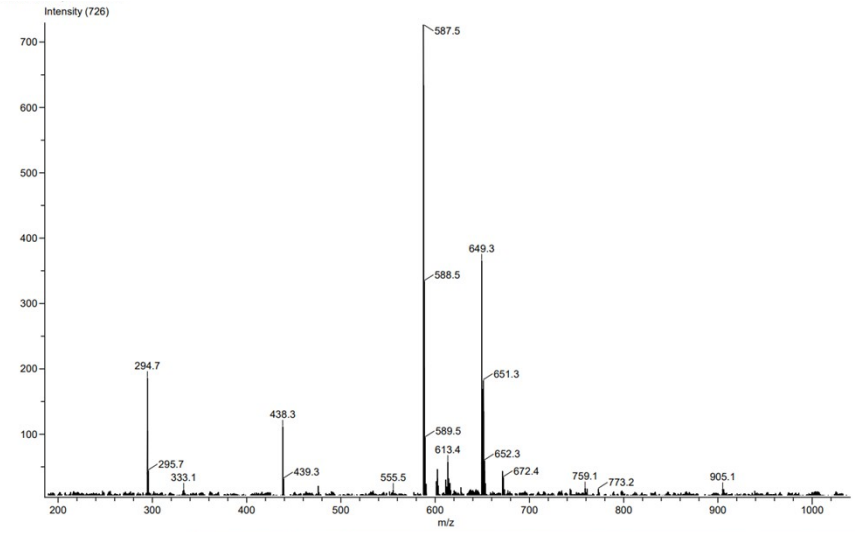

Figure S5: LIFDI mass spectrum of **2**.

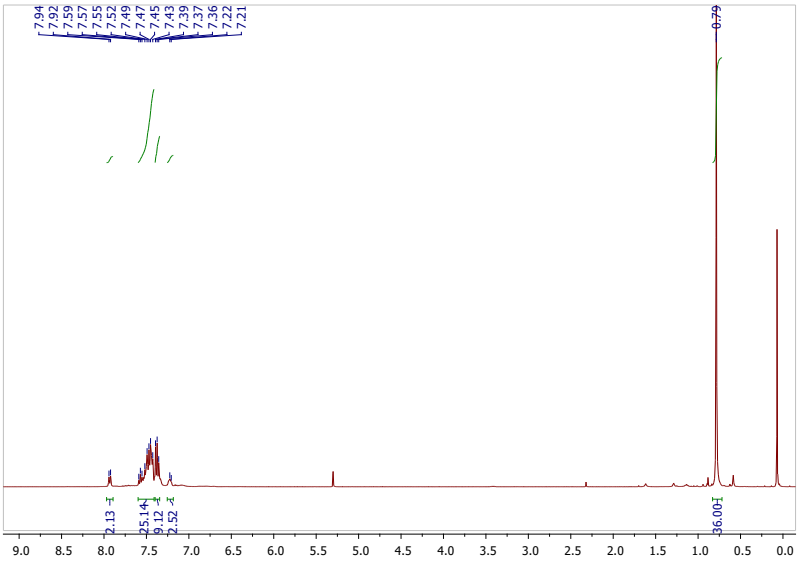

Figure S6: ^{1}H NMR spectrum of **4** at 298 K.

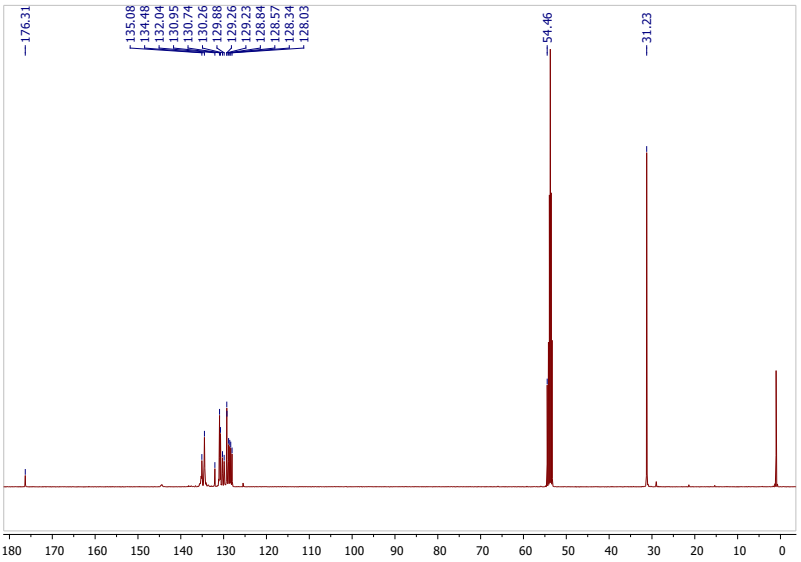

Figure S7: ^{13}C NMR spectrum of **4** at 298 K.

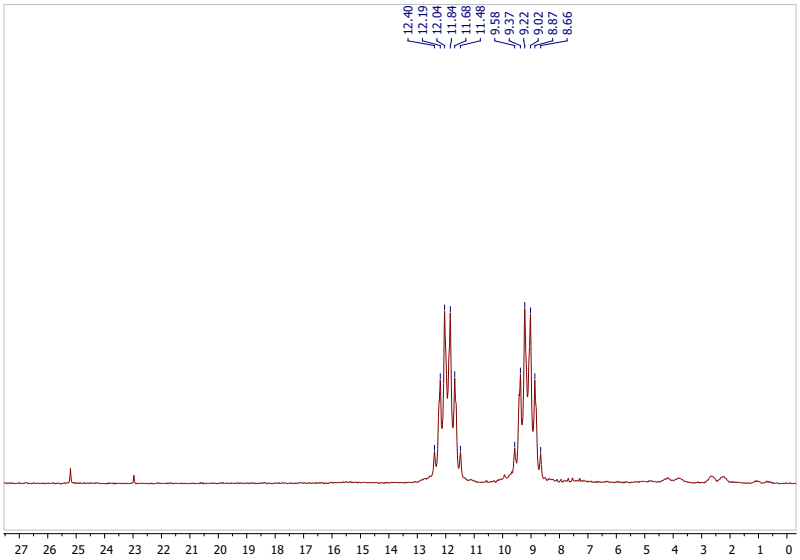

Figure S8: ^{31}P NMR spectrum of **4** at 298 K.

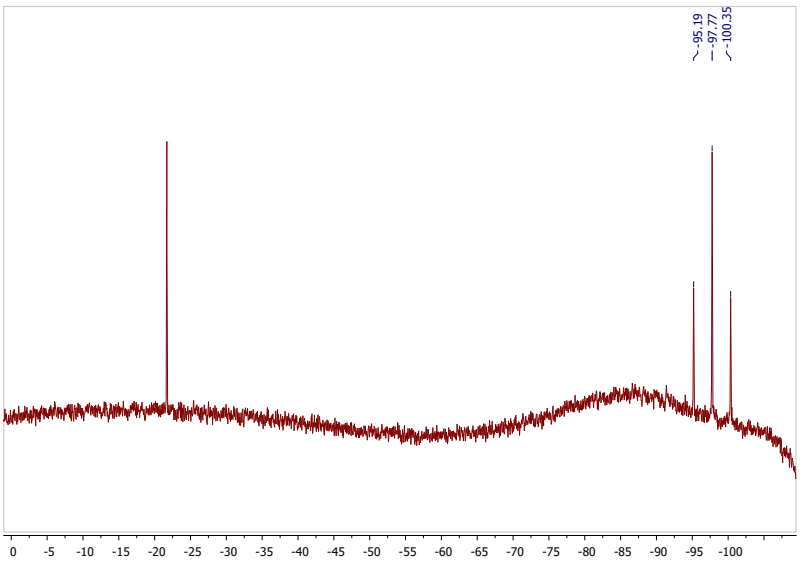

Figure S9: ^{29}Si NMR spectrum of **4** at 298 K.

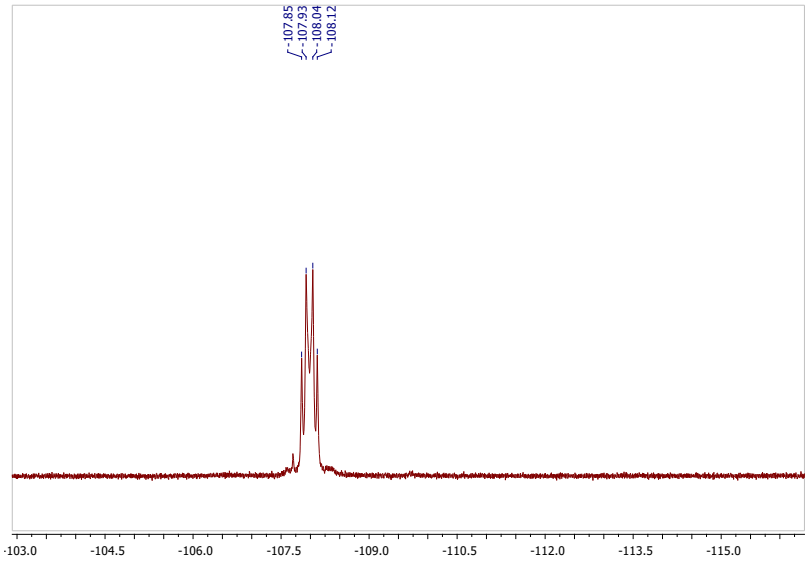

Figure S10: ^{19}F NMR spectrum of **4** at 298 K.

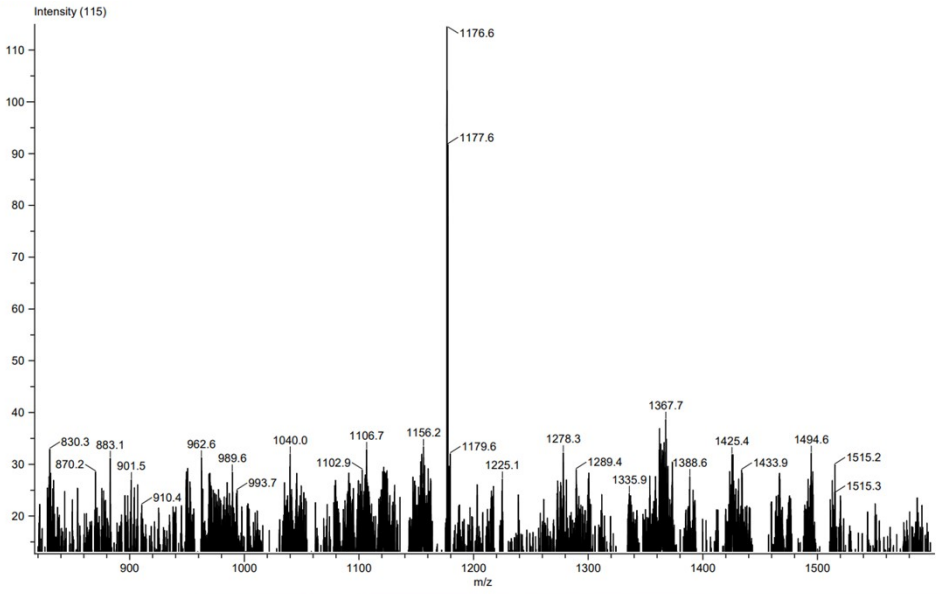

Figure S11-a: LIFDI mass spectrum of **4**.

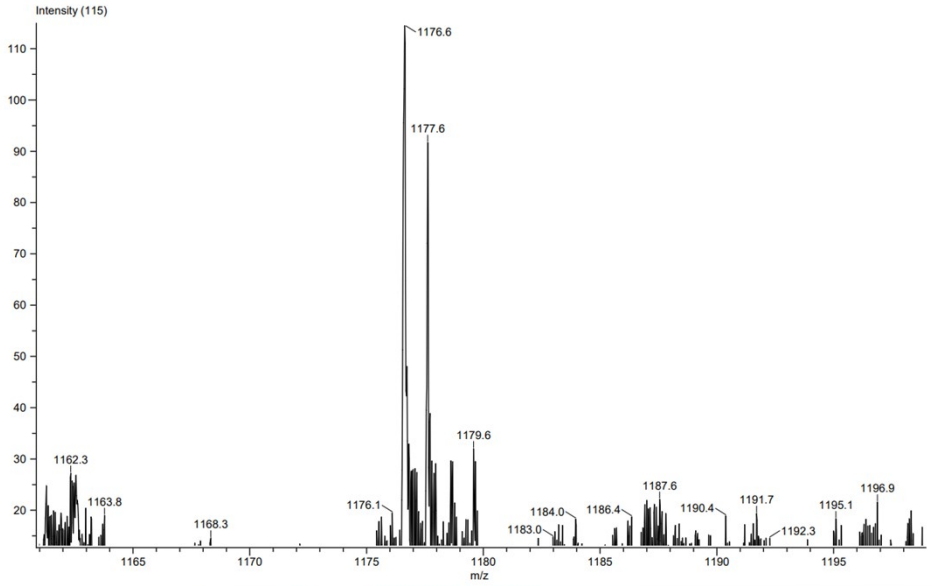

Figure S11-b: LIFDI mass spectrum of **4**.

X-ray crystallographic details

The data were collected from shock-cooled crystals at 100(2) K, on a Bruker D8 three circle diffractometer equipped with an Incoatec Mo Microsource (MoKα radiation, λ = 0.71073 Å). The data were integrated with SAINT. [1] An empirical absorption correction was applied using SADABS[2] (**4**) or TWINABS (**2**).[3] The structures were solved by SHELXT[4] and refined on F^2 using SHELXL[5] in the graphical user interface SHELXLE.[6] All non-hydrogen-atoms were refined with anisotropic displacement parameters. The hydrogen atoms were refined isotropically on calculated positions using a riding model with their U_{iso} values constrained to 1.5 U_{eq} of their pivot atoms for terminal sp^3 carbon atoms and 1.2 times for all other carbon atoms.

Table S1: Crystal data for compounds **2** and **4**.

Compound	**2**	**4**
CCDC	2125569	2125570
Empirical formula	$C_{33}H_{37}Au_2Cl_2N_2P$ Si,0.385(CH_2Cl_2)	$C_{66}H_{74}AgF_4N_4P_2Si_2$, 2($C_7H_8$), 0.923($AlCl_4$), 0.077($F_4Sb$)
Formula weight (g/mol)	1018.21	1580.56
Temperature (K)	100(2)	100(2)
Wavelength (Å)	0.71073	0.71073
Crystal system	Monoclinic	Monoclinic
Space group	$P2_1/n$	$P2_1/c$
a (Å)	9.108(2)	13.773(2)
b (Å)	19.980(3)	13.572(2)
c (Å)	19.558(3)	41.898(6)
β (deg)	99.34(2)	91.83(3)
V (Å^3)	3511.9(11)	7828(2)
Z	4	4
Density (Mg/m3)	1.926	1.341
μ(mm^{-1})	8.661	0.547
Crystal size(mm)		0.188 x 0.164 x 0.153
Crystal color, shape	Block, colourless	Block colourless
Θ range (deg)	1.467 to 26.199	1.479 to 26.423
Reflections collected	137050	146476

Independent reflections	8070	16046
R_{int}	0.1188	0.1034
Data/restraints/parameters	8070 / 776 / 436	16046 / 2110 / 1176
$R1$ ($I > 2\sigma(I)$)	0.0571	0.0478
$wR2$ (all data)	0.1533	0.1259
$\Delta\rho_{max}/\Delta\rho_{min}$(e Å^{-3})	3.039/-2.134	1.275/-1.072

Crystal structure of **2**

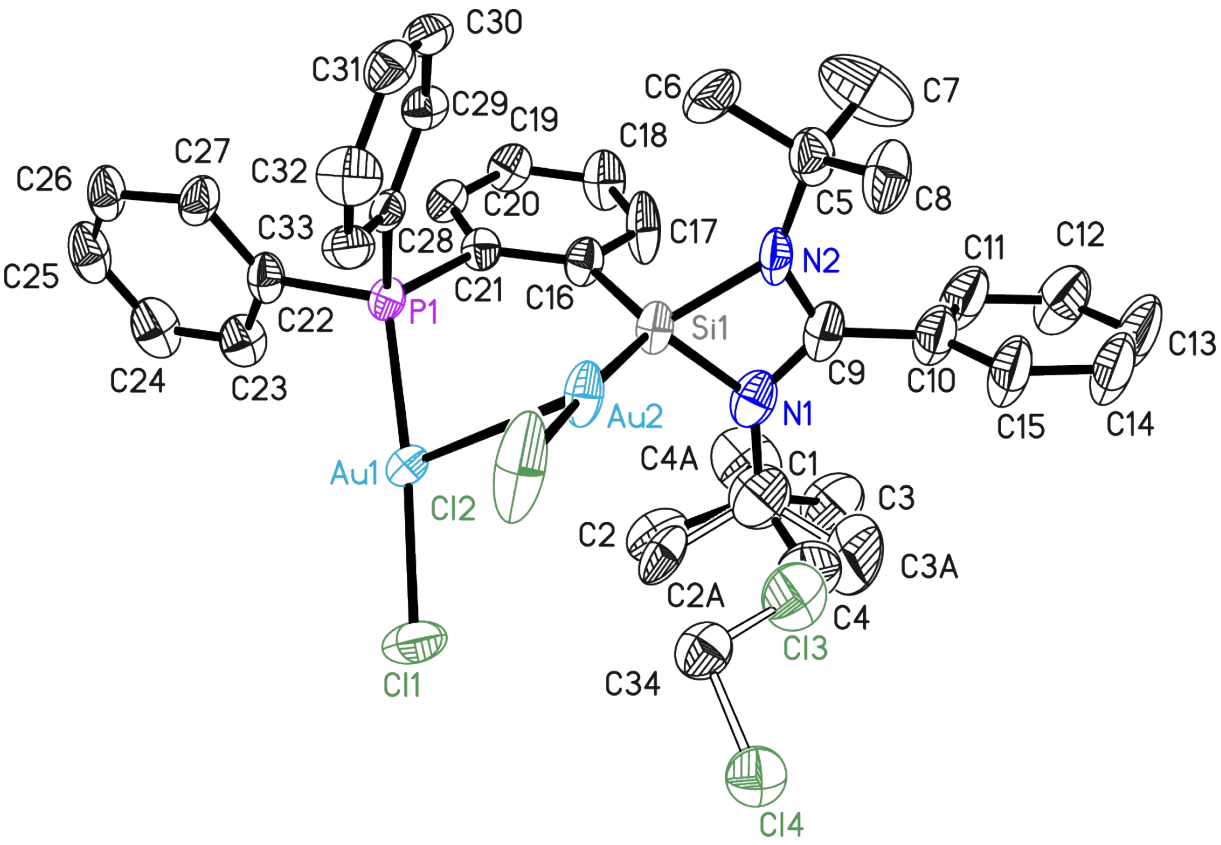

Figure S12 : Crystal structure of **2.** Thermal ellipsoids are represented at the 50% probability level. Hydrogen atoms are omitted

The data were collected on a split crystal treated as a three components twin. The fractional contribution of the minor components refined to 0.205(2) and 0.196(4).

One t-butyl group was disordered over two positions with an occupancy of 0.385(8) for the minor component. The DCM molecule can only be present together with this minor position. All disordered groups are refined with distance restraints and restraints for the anisotropic displacement parameters.

Table S2 : Bond lengths (Å) and angles (°) for **2:**

Au(1)-P(1)	2.228(3)	Si(1)-N(2)	1.812(9)
Au(1)-Cl(1)	2.287(3)	Si(1)-N(1)	1.815(9)
Au(1)-Au(2)	2.9987(7)	Si(1)-C(16)	1.895(11)
Au(2)-Si(1)	2.238(3)	Si(1)-C(9)	2.257(12)
Au(2)-Cl(2)	2.325(4)	C(9)-N(2)	1.323(13)
P(1)-C(28)	1.809(11)	C(9)-N(1)	1.324(13)
P(1)-C(22)	1.821(10)	C(9)-C(10)	1.500(16)
P(1)-C(21)	1.831(11)	N(1)-C(1)	1.464(16)

C(1)-C(3A)	1.477(16)	P(1)-Au(1)-Au(2)	85.25(7)
C(1)-C(3)	1.497(15)	Cl(1)-Au(1)-Au(2)	98.34(10)
C(1)-C(2)	1.500(15)	Si(1)-Au(2)-Cl(2)	173.86(13)
C(1)-C(2A)	1.524(16)	Si(1)-Au(2)-Au(1)	87.18(8)
C(1)-C(4A)	1.593(16)	Cl(2)-Au(2)-Au(1)	98.85(13)
C(1)-C(4)	1.596(15)	C(28)-P(1)-C(22)	105.8(5)
C(5)-N(2)	1.473(15)	C(28)-P(1)-C(21)	105.8(5)
C(5)-C(7)	1.516(13)	C(22)-P(1)-C(21)	105.2(5)
C(5)-C(8)	1.519(12)	C(28)-P(1)-Au(1)	113.2(3)
C(5)-C(6)	1.532(13)	C(22)-P(1)-Au(1)	111.0(4)
C(10)-C(11)	1.359(19)	C(21)-P(1)-Au(1)	115.0(3)
C(10)-C(15)	1.39(2)	N(2)-Si(1)-N(1)	71.7(5)
C(11)-C(12)	1.389(19)	N(2)-Si(1)-C(16)	105.0(5)
C(12)-C(13)	1.37(2)	N(1)-Si(1)-C(16)	105.3(5)
C(13)-C(14)	1.41(2)	N(2)-Si(1)-Au(2)	116.2(4)
C(14)-C(15)	1.356(18)	N(1)-Si(1)-Au(2)	118.9(4)
C(16)-C(17)	1.395(16)	C(16)-Si(1)-Au(2)	126.3(4)
C(16)-C(21)	1.404(14)	N(2)-Si(1)-C(9)	35.9(4)
C(17)-C(18)	1.417(16)	N(1)-Si(1)-C(9)	35.9(4)
C(18)-C(19)	1.354(16)	C(16)-Si(1)-C(9)	110.5(5)
C(19)-C(20)	1.395(16)	Au(2)-Si(1)-C(9)	123.2(3)
C(20)-C(21)	1.385(14)	N(2)-C(9)-N(1)	106.8(10)
C(22)-C(27)	1.387(17)	N(2)-C(9)-C(10)	126.7(11)
C(22)-C(23)	1.394(18)	N(1)-C(9)-C(10)	126.5(11)
C(23)-C(24)	1.390(17)	N(2)-C(9)-Si(1)	53.4(6)
C(24)-C(25)	1.41(2)	N(1)-C(9)-Si(1)	53.5(6)
C(25)-C(26)	1.33(2)	C(10)-C(9)-Si(1)	178.5(10)
C(26)-C(27)	1.412(15)	C(9)-N(1)-C(1)	132.9(9)
C(28)-C(29)	1.381(15)	C(9)-N(1)-Si(1)	90.6(7)
C(28)-C(33)	1.390(15)	C(1)-N(1)-Si(1)	135.4(8)
C(29)-C(30)	1.375(16)	N(1)-C(1)-C(3A)	121.0(18)
C(30)-C(31)	1.386(16)	N(1)-C(1)-C(3)	115.7(14)
C(31)-C(32)	1.367(18)	N(1)-C(1)-C(2)	109.7(14)
C(32)-C(33)	1.377(18)	C(3)-C(1)-C(2)	118.2(16)
C(34)-Cl(4)	1.73(3)	N(1)-C(1)-C(2A)	110.6(16)
C(34)-Cl(3)	1.75(4)	C(3A)-C(1)-C(2A)	116.8(19)
		N(1)-C(1)-C(4A)	99.8(14)
P(1)-Au(1)-Cl(1)	175.42(12)	C(3A)-C(1)-C(4A)	104.4(17)

C(2A)-C(1)-C(4A)	99.9(16)	C(16)-C(17)-C(18)	121.9(10)
N(1)-C(1)-C(4)	104.1(13)	C(19)-C(18)-C(17)	119.7(11)
C(3)-C(1)-C(4)	101.9(14)	C(18)-C(19)-C(20)	119.3(11)
C(2)-C(1)-C(4)	105.4(14)	C(21)-C(20)-C(19)	121.6(10)
N(2)-C(5)-C(7)	111.1(11)	C(20)-C(21)-C(16)	120.3(10)
N(2)-C(5)-C(8)	110.6(10)	C(20)-C(21)-P(1)	118.4(8)
C(7)-C(5)-C(8)	110.9(11)	C(16)-C(21)-P(1)	121.3(8)
N(2)-C(5)-C(6)	107.2(9)	C(27)-C(22)-C(23)	121.1(10)
C(7)-C(5)-C(6)	108.2(12)	C(27)-C(22)-P(1)	120.5(9)
C(8)-C(5)-C(6)	108.7(10)	C(23)-C(22)-P(1)	118.4(9)
C(9)-N(2)-C(5)	133.5(9)	C(24)-C(23)-C(22)	119.8(13)
C(9)-N(2)-Si(1)	90.7(7)	C(23)-C(24)-C(25)	118.6(14)
C(5)-N(2)-Si(1)	135.5(7)	C(26)-C(25)-C(24)	120.9(11)
C(11)-C(10)-C(15)	120.2(12)	C(25)-C(26)-C(27)	121.7(13)
C(11)-C(10)-C(9)	120.3(12)	C(22)-C(27)-C(26)	117.7(13)
C(15)-C(10)-C(9)	119.3(12)	C(29)-C(28)-C(33)	119.0(10)
C(10)-C(11)-C(12)	120.0(14)	C(29)-C(28)-P(1)	121.9(8)
C(13)-C(12)-C(11)	119.6(15)	C(33)-C(28)-P(1)	119.1(8)
C(12)-C(13)-C(14)	120.5(14)	C(30)-C(29)-C(28)	120.5(11)
C(15)-C(14)-C(13)	118.9(15)	C(29)-C(30)-C(31)	119.9(11)
C(14)-C(15)-C(10)	120.7(15)	C(32)-C(31)-C(30)	120.0(11)
C(17)-C(16)-C(21)	117.0(10)	C(31)-C(32)-C(33)	120.3(12)
C(17)-C(16)-Si(1)	115.1(8)	C(32)-C(33)-C(28)	120.3(11)
C(21)-C(16)-Si(1)	127.8(8)	Cl(4)-C(34)-Cl(3)	112.2(18)

Crystal structure of **4**

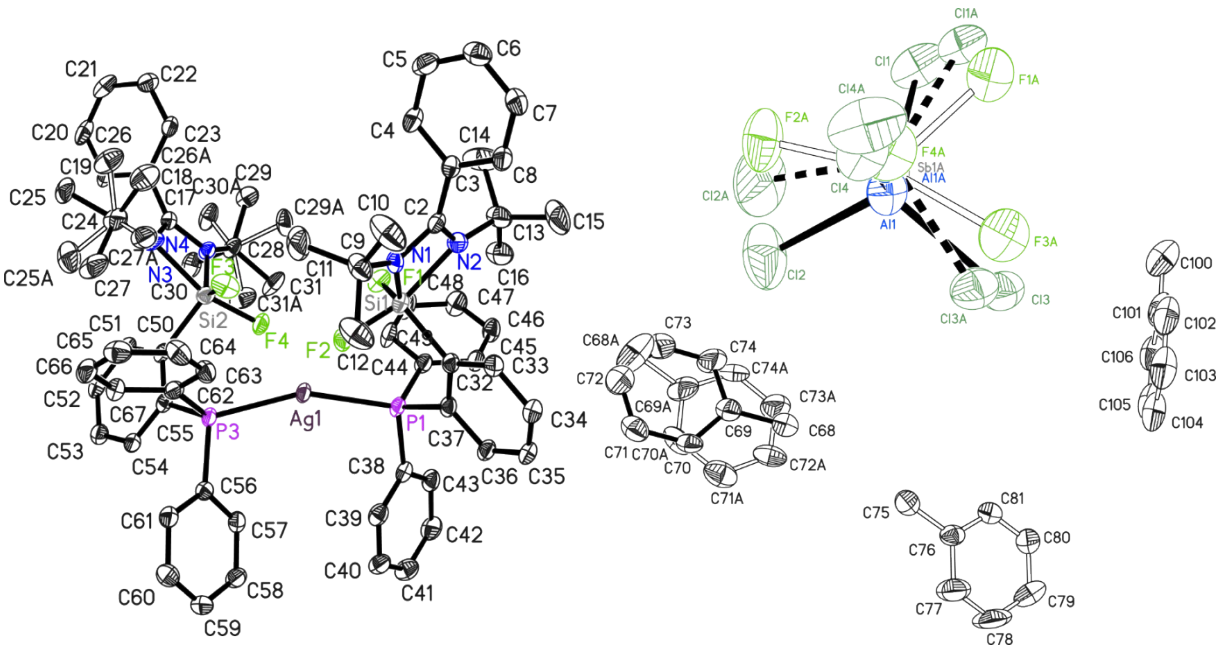

Figure S13. Crystal structure of **4** (left cation, top right anion, bottom right solvent). Thermal ellipsoids are represented at the 50% probability level. Hydrogen atoms are omitted

The asymmetric unit contains of one cation, one anion and one and two half toluene molecules. One toluene molecule is disordered over two positions with occupancies of 0.695(6) and 0.305(6), while the two half toluene molecules are disordered about inversion centers. The anion is disordered over two positions of $AlCl_4^-$ (occupancies of 0.529(3) and 0.394(3)) and one SbF_4^- ion with occupancy of 0.0771(14). In the cation two t-butyl groups are disordered over two positions with an occupancy of the minor components of 0.198(6) and 0.479(6). All disordered groups are refined with distance restraints and restraints for the anisotropic displacement parameters.

Table S3 : Bond lengths (Å) and angles (°) for **4:**

Ag(1)-P(3)	2.4291(8)	Al(1A)-Cl(1A)	2.116(10)
Ag(1)-P(1)	2.4350(10)	Al(1A)-Cl(2A)	2.131(9)
Al(1)-Cl(4)	2.131(8)	Al(1A)-Cl(3A)	2.152(10)
Al(1)-Cl(3)	2.136(8)	P(1)-C(44)	1.818(3)
Al(1)-Cl(1)	2.137(6)	P(1)-C(38)	1.824(3)
Al(1)-Cl(2)	2.137(8)	P(1)-C(37)	1.841(3)
Sb(1A)-F(2A)	1.84(3)	Si(1)-F(1)	1.606(2)
Sb(1A)-F(3A)	1.86(3)	Si(1)-F(2)	1.6577(19)
Sb(1A)-F(1A)	1.99(3)	Si(1)-N(1)	1.801(3)
Sb(1A)-F(4A)	1.99(3)	Si(1)-C(32)	1.880(3)
Al(1A)-Cl(4A)	2.113(10)	Si(1)-N(2)	1.976(3)

Si(1)-C(2)	2.354(3)	C(24)-C(26A)	1.458(11)
N(1)-C(2)	1.366(4)	C(24)-C(25A)	1.494(11)
N(1)-C(9)	1.493(4)	C(24)-C(27)	1.495(5)
Si(2)-F(3)	1.606(2)	C(24)-C(26)	1.497(6)
Si(2)-F(4)	1.654(2)	C(24)-C(25)	1.596(5)
Si(2)-N(4)	1.823(3)	C(24)-C(27A)	1.643(11)
Si(2)-C(50)	1.883(3)	C(28)-C(30A)	1.483(7)
Si(2)-N(3)	1.951(3)	C(28)-C(31)	1.494(6)
Si(2)-C(17)	2.346(3)	C(28)-C(31A)	1.498(7)
N(2)-C(2)	1.308(4)	C(28)-C(29)	1.500(6)
N(2)-C(13)	1.486(4)	C(28)-C(29A)	1.603(7)
C(2)-C(3)	1.484(5)	C(28)-C(30)	1.613(7)
P(3)-C(62)	1.822(3)	C(32)-C(33)	1.398(4)
P(3)-C(56)	1.830(3)	C(32)-C(37)	1.417(4)
P(3)-C(55)	1.844(3)	C(33)-C(34)	1.391(5)
C(3)-C(8)	1.383(5)	C(34)-C(35)	1.377(5)
C(3)-C(4)	1.403(5)	C(35)-C(36)	1.380(5)
N(4)-C(17)	1.355(4)	C(36)-C(37)	1.405(4)
N(4)-C(28)	1.492(4)	C(38)-C(43)	1.394(4)
C(4)-C(5)	1.382(5)	C(38)-C(39)	1.395(4)
C(5)-C(6)	1.387(5)	C(39)-C(40)	1.386(5)
C(6)-C(7)	1.384(5)	C(40)-C(41)	1.391(5)
C(7)-C(8)	1.383(5)	C(41)-C(42)	1.377(5)
C(9)-C(11)	1.523(5)	C(42)-C(43)	1.382(5)
C(9)-C(12)	1.526(5)	C(44)-C(49)	1.394(4)
C(9)-C(10)	1.526(5)	C(44)-C(45)	1.398(4)
C(13)-C(15)	1.522(6)	C(45)-C(46)	1.384(5)
C(13)-C(16)	1.528(5)	C(46)-C(47)	1.388(5)
C(13)-C(14)	1.529(5)	C(47)-C(48)	1.380(5)
C(17)-N(3)	1.302(4)	C(48)-C(49)	1.383(5)
C(17)-C(18)	1.495(4)	C(50)-C(55)	1.413(4)
C(18)-C(23)	1.380(5)	C(50)-C(51)	1.413(4)
C(18)-C(19)	1.393(5)	C(51)-C(52)	1.378(5)
C(19)-C(20)	1.393(5)	C(52)-C(53)	1.386(5)
C(20)-C(21)	1.372(5)	C(53)-C(54)	1.385(4)
C(21)-C(22)	1.379(5)	C(54)-C(55)	1.395(4)
C(22)-C(23)	1.393(5)	C(56)-C(57)	1.392(4)
N(3)-C(24)	1.488(4)	C(56)-C(61)	1.394(4)

C(57)-C(58)	1.384(4)		
C(58)-C(59)	1.389(5)	P(3)-Ag(1)-P(1)	157.06(3)
C(59)-C(60)	1.375(5)	Cl(4)-Al(1)-Cl(3)	112.8(4)
C(60)-C(61)	1.392(5)	Cl(4)-Al(1)-Cl(1)	107.1(4)
C(62)-C(63)	1.381(5)	Cl(3)-Al(1)-Cl(1)	108.7(4)
C(62)-C(67)	1.397(5)	Cl(4)-Al(1)-Cl(2)	110.2(4)
C(63)-C(64)	1.392(5)	Cl(3)-Al(1)-Cl(2)	106.2(4)
C(64)-C(65)	1.384(5)	Cl(1)-Al(1)-Cl(2)	111.8(3)
C(65)-C(66)	1.376(5)	F(2A)-Sb(1A)-F(3A)	163(2)
C(66)-C(67)	1.385(5)	F(2A)-Sb(1A)-F(1A)	123(2)
C(68)-C(69)	1.497(8)	F(3A)-Sb(1A)-F(1A)	73.6(17)
C(69)-C(70)	1.370(8)	F(2A)-Sb(1A)-F(4A)	97.3(19)
C(69)-C(74)	1.418(8)	F(3A)-Sb(1A)-F(4A)	85.4(17)
C(70)-C(71)	1.389(8)	F(1A)-Sb(1A)-F(4A)	93(2)
C(71)-C(72)	1.344(8)	Cl(4A)-Al(1A)-Cl(1A)	106.6(5)
C(72)-C(73)	1.403(9)	Cl(4A)-Al(1A)-Cl(2A)	110.2(6)
C(73)-C(74)	1.358(9)	Cl(1A)-Al(1A)-Cl(2A)	112.0(5)
C(68A)-C(69A)	1.495(14)	Cl(4A)-Al(1A)-Cl(3A)	110.6(6)
C(69A)-C(70A)	1.365(12)	Cl(1A)-Al(1A)-Cl(3A)	109.5(6)
C(69A)-C(74A)	1.412(12)	Cl(2A)-Al(1A)-Cl(3A)	107.9(5)
C(70A)-C(71A)	1.361(12)	C(44)-P(1)-C(38)	104.20(15)
C(71A)-C(72A)	1.353(12)	C(44)-P(1)-C(37)	105.66(14)
C(72A)-C(73A)	1.364(12)	C(38)-P(1)-C(37)	104.11(14)
C(73A)-C(74A)	1.379(12)	C(44)-P(1)-Ag(1)	114.88(11)
C(75)-C(76)	1.508(10)	C(38)-P(1)-Ag(1)	108.13(11)
C(76)-C(77)	1.369(10)	C(37)-P(1)-Ag(1)	118.46(10)
C(76)-C(81)	1.391(10)	F(1)-Si(1)-F(2)	92.15(11)
C(77)-C(78)	1.373(11)	F(1)-Si(1)-N(1)	123.25(12)
C(78)-C(79)	1.368(11)	F(2)-Si(1)-N(1)	95.27(11)
C(79)-C(80)	1.369(10)	F(1)-Si(1)-C(32)	115.68(12)
C(80)-C(81)	1.360(10)	F(2)-Si(1)-C(32)	97.65(12)
C(100)-C(101)	1.489(13)	N(1)-Si(1)-C(32)	118.83(14)
C(101)-C(106)	1.381(11)	F(1)-Si(1)-N(2)	90.38(12)
C(101)-C(102)	1.388(11)	F(2)-Si(1)-N(2)	162.32(11)
C(102)-C(103)	1.361(11)	N(1)-Si(1)-N(2)	68.90(12)
C(103)-C(104)	1.385(11)	C(32)-Si(1)-N(2)	96.99(13)
C(104)-C(105)	1.344(11)	F(1)-Si(1)-C(2)	107.17(11)
C(105)-C(106)	1.382(11)	F(2)-Si(1)-C(2)	129.58(11)

N(1)-Si(1)-C(2)	35.30(11)	C(4)-C(3)-C(2)	118.1(3)
C(32)-Si(1)-C(2)	113.49(13)	C(17)-N(4)-C(28)	128.4(2)
N(2)-Si(1)-C(2)	33.74(11)	C(17)-N(4)-Si(2)	93.96(19)
C(2)-N(1)-C(9)	130.1(3)	C(28)-N(4)-Si(2)	137.2(2)
C(2)-N(1)-Si(1)	95.1(2)	C(5)-C(4)-C(3)	119.4(3)
C(9)-N(1)-Si(1)	134.8(2)	C(4)-C(5)-C(6)	120.7(3)
F(3)-Si(2)-F(4)	91.36(11)	C(7)-C(6)-C(5)	119.6(3)
F(3)-Si(2)-N(4)	128.37(12)	C(8)-C(7)-C(6)	120.3(3)
F(4)-Si(2)-N(4)	95.45(11)	C(3)-C(8)-C(7)	120.2(3)
F(3)-Si(2)-C(50)	114.99(13)	N(1)-C(9)-C(11)	107.8(3)
F(4)-Si(2)-C(50)	97.31(12)	N(1)-C(9)-C(12)	108.7(3)
N(4)-Si(2)-C(50)	114.72(13)	C(11)-C(9)-C(12)	110.3(3)
F(3)-Si(2)-N(3)	90.50(13)	N(1)-C(9)-C(10)	113.0(3)
F(4)-Si(2)-N(3)	161.03(12)	C(11)-C(9)-C(10)	109.7(3)
N(4)-Si(2)-N(3)	68.88(12)	C(12)-C(9)-C(10)	107.4(3)
C(50)-Si(2)-N(3)	98.99(13)	N(2)-C(13)-C(15)	110.0(3)
F(3)-Si(2)-C(17)	111.35(12)	N(2)-C(13)-C(16)	106.0(3)
F(4)-Si(2)-C(17)	129.64(11)	C(15)-C(13)-C(16)	108.4(3)
N(4)-Si(2)-C(17)	35.20(11)	N(2)-C(13)-C(14)	111.4(3)
C(50)-Si(2)-C(17)	110.97(13)	C(15)-C(13)-C(14)	111.4(4)
N(3)-Si(2)-C(17)	33.70(11)	C(16)-C(13)-C(14)	109.4(3)
C(2)-N(2)-C(13)	129.4(3)	N(3)-C(17)-N(4)	107.1(3)
C(2)-N(2)-Si(1)	89.2(2)	N(3)-C(17)-C(18)	124.8(3)
C(13)-N(2)-Si(1)	140.5(2)	N(4)-C(17)-C(18)	128.1(3)
N(2)-C(2)-N(1)	106.4(3)	N(3)-C(17)-Si(2)	56.25(17)
N(2)-C(2)-C(3)	127.3(3)	N(4)-C(17)-Si(2)	50.84(14)
N(1)-C(2)-C(3)	126.2(3)	C(18)-C(17)-Si(2)	178.0(2)
N(2)-C(2)-Si(1)	57.06(17)	C(23)-C(18)-C(19)	119.8(3)
N(1)-C(2)-Si(1)	49.64(15)	C(23)-C(18)-C(17)	119.4(3)
C(3)-C(2)-Si(1)	171.1(2)	C(19)-C(18)-C(17)	120.6(3)
C(62)-P(3)-C(56)	102.73(14)	C(20)-C(19)-C(18)	119.4(3)
C(62)-P(3)-C(55)	104.80(14)	C(21)-C(20)-C(19)	120.5(3)
C(56)-P(3)-C(55)	104.70(14)	C(20)-C(21)-C(22)	120.3(3)
C(62)-P(3)-Ag(1)	115.07(11)	C(21)-C(22)-C(23)	119.7(3)
C(56)-P(3)-Ag(1)	108.49(11)	C(18)-C(23)-C(22)	120.3(3)
C(55)-P(3)-Ag(1)	119.37(10)	C(17)-N(3)-C(24)	130.6(3)
C(8)-C(3)-C(4)	119.8(3)	C(17)-N(3)-Si(2)	90.1(2)
C(8)-C(3)-C(2)	122.0(3)	C(24)-N(3)-Si(2)	137.3(2)

C(26A)-C(24)-N(3)	119.6(8)	C(39)-C(40)-C(41)	119.6(3)
C(26A)-C(24)-C(25A)	123.2(11)	C(42)-C(41)-C(40)	119.7(3)
N(3)-C(24)-C(25A)	102.2(8)	C(41)-C(42)-C(43)	120.8(3)
N(3)-C(24)-C(27)	107.7(3)	C(42)-C(43)-C(38)	120.2(3)
N(3)-C(24)-C(26)	109.1(3)	C(49)-C(44)-C(45)	119.3(3)
C(27)-C(24)-C(26)	113.7(4)	C(49)-C(44)-P(1)	118.4(2)
N(3)-C(24)-C(25)	112.2(3)	C(45)-C(44)-P(1)	122.3(2)
C(27)-C(24)-C(25)	106.7(4)	C(46)-C(45)-C(44)	120.1(3)
C(26)-C(24)-C(25)	107.5(3)	C(45)-C(46)-C(47)	120.3(3)
C(26A)-C(24)-C(27A)	103.2(9)	C(48)-C(47)-C(46)	119.7(3)
N(3)-C(24)-C(27A)	103.8(7)	C(47)-C(48)-C(49)	120.6(3)
C(25A)-C(24)-C(27A)	101.9(10)	C(48)-C(49)-C(44)	120.1(3)
C(30A)-C(28)-N(4)	116.4(4)	C(55)-C(50)-C(51)	116.5(3)
N(4)-C(28)-C(31)	113.2(4)	C(55)-C(50)-Si(2)	127.4(2)
C(30A)-C(28)-C(31A)	112.3(5)	C(51)-C(50)-Si(2)	115.9(2)
N(4)-C(28)-C(31A)	110.5(4)	C(52)-C(51)-C(50)	122.5(3)
N(4)-C(28)-C(29)	114.0(3)	C(51)-C(52)-C(53)	120.0(3)
C(31)-C(28)-C(29)	111.7(5)	C(54)-C(53)-C(52)	119.2(3)
C(30A)-C(28)-C(29A)	107.0(5)	C(53)-C(54)-C(55)	121.3(3)
N(4)-C(28)-C(29A)	102.2(3)	C(54)-C(55)-C(50)	120.5(3)
C(31A)-C(28)-C(29A)	107.5(5)	C(54)-C(55)-P(3)	118.2(2)
N(4)-C(28)-C(30)	105.0(3)	C(50)-C(55)-P(3)	121.3(2)
C(31)-C(28)-C(30)	105.3(5)	C(57)-C(56)-C(61)	119.2(3)
C(29)-C(28)-C(30)	106.8(4)	C(57)-C(56)-P(3)	118.0(2)
C(33)-C(32)-C(37)	117.5(3)	C(61)-C(56)-P(3)	122.9(2)
C(33)-C(32)-Si(1)	115.5(2)	C(58)-C(57)-C(56)	120.6(3)
C(37)-C(32)-Si(1)	126.9(2)	C(57)-C(58)-C(59)	119.9(3)
C(34)-C(33)-C(32)	122.2(3)	C(60)-C(59)-C(58)	119.9(3)
C(35)-C(34)-C(33)	119.5(3)	C(59)-C(60)-C(61)	120.6(3)
C(34)-C(35)-C(36)	120.2(3)	C(60)-C(61)-C(56)	119.8(3)
C(35)-C(36)-C(37)	120.9(3)	C(63)-C(62)-C(67)	119.6(3)
C(36)-C(37)-C(32)	119.6(3)	C(63)-C(62)-P(3)	118.8(2)
C(36)-C(37)-P(1)	118.7(2)	C(67)-C(62)-P(3)	121.5(2)
C(32)-C(37)-P(1)	121.6(2)	C(62)-C(63)-C(64)	120.3(3)
C(43)-C(38)-C(39)	118.7(3)	C(65)-C(64)-C(63)	119.7(3)
C(43)-C(38)-P(1)	124.0(2)	C(66)-C(65)-C(64)	120.4(3)
C(39)-C(38)-P(1)	117.3(2)	C(65)-C(66)-C(67)	120.2(3)
C(40)-C(39)-C(38)	120.9(3)	C(66)-C(67)-C(62)	119.9(3)

C(70)-C(69)-C(74)	116.7(6)	C(77)-C(76)-C(81)	116.3(8)
C(70)-C(69)-C(68)	122.6(6)	C(77)-C(76)-C(75)	120.6(8)
C(74)-C(69)-C(68)	120.6(6)	C(81)-C(76)-C(75)	122.8(7)
C(69)-C(70)-C(71)	121.7(6)	C(76)-C(77)-C(78)	121.7(9)
C(72)-C(71)-C(70)	121.6(6)	C(79)-C(78)-C(77)	120.6(10)
C(71)-C(72)-C(73)	117.9(7)	C(78)-C(79)-C(80)	118.9(9)
C(74)-C(73)-C(72)	121.4(7)	C(81)-C(80)-C(79)	120.0(9)
C(73)-C(74)-C(69)	120.7(7)	C(80)-C(81)-C(76)	122.3(9)
C(70A)-C(69A)-C(74A)	116.6(11)	C(106)-C(101)-C(102)	118.3(9)
C(70A)-C(69A)-C(68A)	120.7(14)	C(106)-C(101)-C(100)	119.0(11)
C(74A)-C(69A)-C(68A)	122.6(14)	C(102)-C(101)-C(100)	122.8(11)
C(71A)-C(70A)-C(69A)	122.7(14)	C(103)-C(102)-C(101)	120.4(10)
C(72A)-C(71A)-C(70A)	120.3(13)	C(102)-C(103)-C(104)	121.1(11)
C(71A)-C(72A)-C(73A)	118.9(12)	C(105)-C(104)-C(103)	118.7(11)
C(72A)-C(73A)-C(74A)	121.1(13)	C(104)-C(105)-C(106)	121.5(11)
C(73A)-C(74A)-C(69A)	119.6(12)	C(101)-C(106)-C(105)	120.1(10)

Computational analysis

Computational details

Geometry optimizations without symmetry restriction were carried out with the Gaussian program[7]. Specifically, geometry optimization was firstly performed at the BP86[8]/def2-TZVP[9] level with Grimme's D3 dispersion corrections,[10] and the solvation effect of the experimentally used toluene was also considered with the SMD solvent model.[11] Included Vibrational frequency calculations were performed for all stationary points to identify whether they were local minima (no imaginary frequencies). The weak interaction analysis was prepared Multiwfn.[12] The Laplacian of the electron density is estimated by the Bader's quantum theory of atoms-in-moleculess (QTAIM)[13] method with the AIMALL[14] program. The structures were illustrated by CYLview20.[15]

The bonding situation was analyzed by means of an energy decomposition analysis (EDA)[16] together with the natural orbitals for chemical valence (NOCV)[17] method by using the ADF 2019.10.3 program package.[18] The EDA-NOCV calculations were carried out at the BP86-D3(BJ)/TZ2P level. In this analysis, the intrinsic interaction energy (ΔE_{int}) between two fragments can be divided into four energy components as follows:

$$\Delta E_{\text{int}} = \Delta E_{\text{elstat}} + \Delta E_{\text{Pauli}} + \Delta E_{\text{orb}} + \Delta E_{\text{disp}} \qquad (1).$$

While the electrostatic ΔE_{elstat} term represents the quasi-classical electrostatic interaction between the unperturbed charge distributions of the prepared fragments, the Pauli repulsion ΔE_{Pauli} corresponds to the energy change associated with the transformation from the superposition of the unperturbed electron densities of the isolated fragments to the wavefunction,[19] which properly obeys the Pauli principle through explicit antisymmetrization and renormalization of the production wavefunction. The orbital term ΔE_{orb} can be further decomposed into contributions from each irreducible representation of the point group of the interacting system as follows:

$$\Delta E_{orb} = \sum_{r} \Delta E_{r} \qquad (2)$$

The combination of the EDA with NOCV enables the partition of the total orbital interactions into pairwise contributions of the orbital interactions which is very vital to get a complete picture of the bonding. The charge deformation $\Delta\rho_k(r)$, resulting from the mixing of the orbital pairs $\psi_k(r)$ and $\psi_{-k}(r)$ of the interacting fragments presents the amount and the shape of the charge flow due to the orbital interactions [Eq. (3)], and the associated energy term ΔE_{orb} provides with the size of stabilizing orbital energy originated from such interaction [Eq. (4)].

$$\Delta\rho_{orb}(r) = \sum_{k} \Delta\rho_{k}(r) = \sum_{k=1}^{N/2} \nu_k [-\psi_{-k}^{2}(r) + \psi_{k}^{2}(r)] \qquad (3)$$

$$\Delta E_{orb} = \sum_{k} \Delta E_{k}^{orb} = \sum_{k=1}^{N/2} \nu_k [-F_{-k,-k}^{TS} + F_{k,k}^{TS}] \qquad (4)$$

More details about the EDA-NOCV method and its application are given in recent review articles.[20]

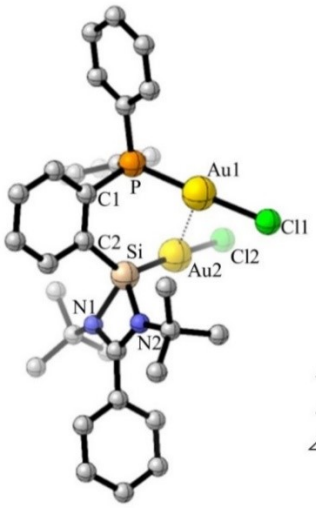

P-Au1=2.249[2.227]
Si-Au2=2.255[2.238]
Au1-Au2=3.039[2.999]
Au1-Cl1=2.318[2.288]
Au1-Cl2=2.353[2.325]
Si-N1=1.843[1.811]
Si-N2=1.839[1.813]
∠C1-P-Au1=112.7[115.1]
∠P-Au1-Cl1=174.7[175.4]
∠C2-Si-Au2=128.6[126.3]
∠Si-Au2-Cl2=173.5[173.9]

ΔE(S) = 0.0 kcal/mol
ΔE(T) = 51.3 kcal/mol

Figure S14. Optimized geometry of complex **2** and the respective fragments at the BP86+(D3BJ)/def2-TZVP (SMD, solvent toluene) level. Selected bond lengths in Å and the angles in degree, the experimental bonds are compared in parentheses. Hydrogen atoms are omitted by clarity (color code, C: gray, P: orange, Au: yellow, Cl: green, Si: brown, N: blue).

Table S4. EDA-NOCV results of complex **2** by using interacting fragments **1** and 2AuCl in their singlet (S), doubled(D) or triplet(T) states at P86+(D3BJ)/TZ2P level of theory. Energy values are given in kcal/mol.

Fragments	**1 (S) + 2AuCl(S)**	**1 (T) + 2AuCl(T)**	**1^{+}(D) + $2AuCl^{-}$(D)**	**1^{-}(D) + $2AuCl^{+}$(D)**	**1^{2-}(S) + $2AuCl^{2+}$(S)**
ΔE_{int}	-173.3	-362.6	-225.9	-390.2	-956.9
ΔE_{Pauli}	437.6	450.9	523.0	444.1	459.1
ΔE_{elstat}[a]	-405.4(66.3%)	-354.2(44.5%)	-435.2(58.1%)	-485.5(58.2%)	-650.6(45.9%)
ΔE_{disp}[a]	-35.1(5.7%)	-35.1(4.3%)	-35.1(4.7%)	-35.1(4.2%)	-35.1(2.5%)
ΔE_{orb}[a]	-170.4(27.8%)	-424.3(52.2%)	-278.6(37.2%)	-313.6(37.6%)	-730.2(51.6%)
ΔE_{orb1}[b]	-58.0(34.0%)				
ΔE_{orb2}[b]	-44.2(25.9%)				
ΔE_{orb3}[b]	-31.6(18.6%)				
$\Delta E_{orb(rest)}$[b]	-36.6 (21.5%)				

[a]The values in parentheses give the percentage contribution to the total attractive interactions $\Delta E_{elstat} + \Delta E_{orb} + \Delta E_{disp}$.

[b]The values in parentheses give the percentage contribution to the total orbital interactions ΔE_{orb}.

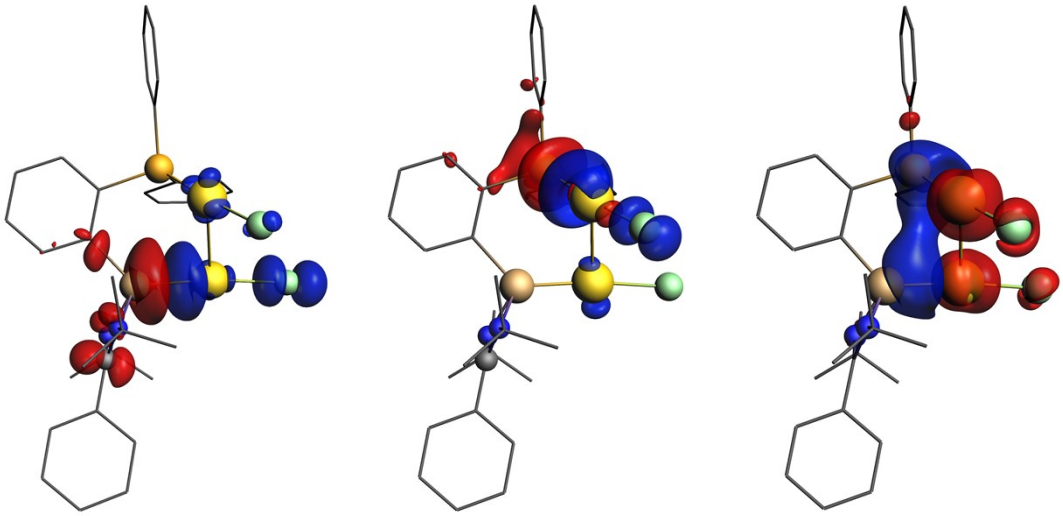

Δρ1
ΔE_{orb1} = - 58.0
ν_1 = ± 0.794

Δρ2
ΔE_{orb2} = - 44.2
ν_2 = ± 0.680

Δρ3
ΔE_{orb3} = - 31.6
ν_3 = ± 0.881

Figure S15. The plot of deformation densities (Δρ) of the pairwise orbital interactions in **2** between the interacting **1** and 2AuCl fragments, with the associated interaction energies (ΔE_{orb}) in kcal/mol. The charge eigenvalues (ν) provide an estimate of the relative size of the charge migration. The direction of charge flow is from red to blue.

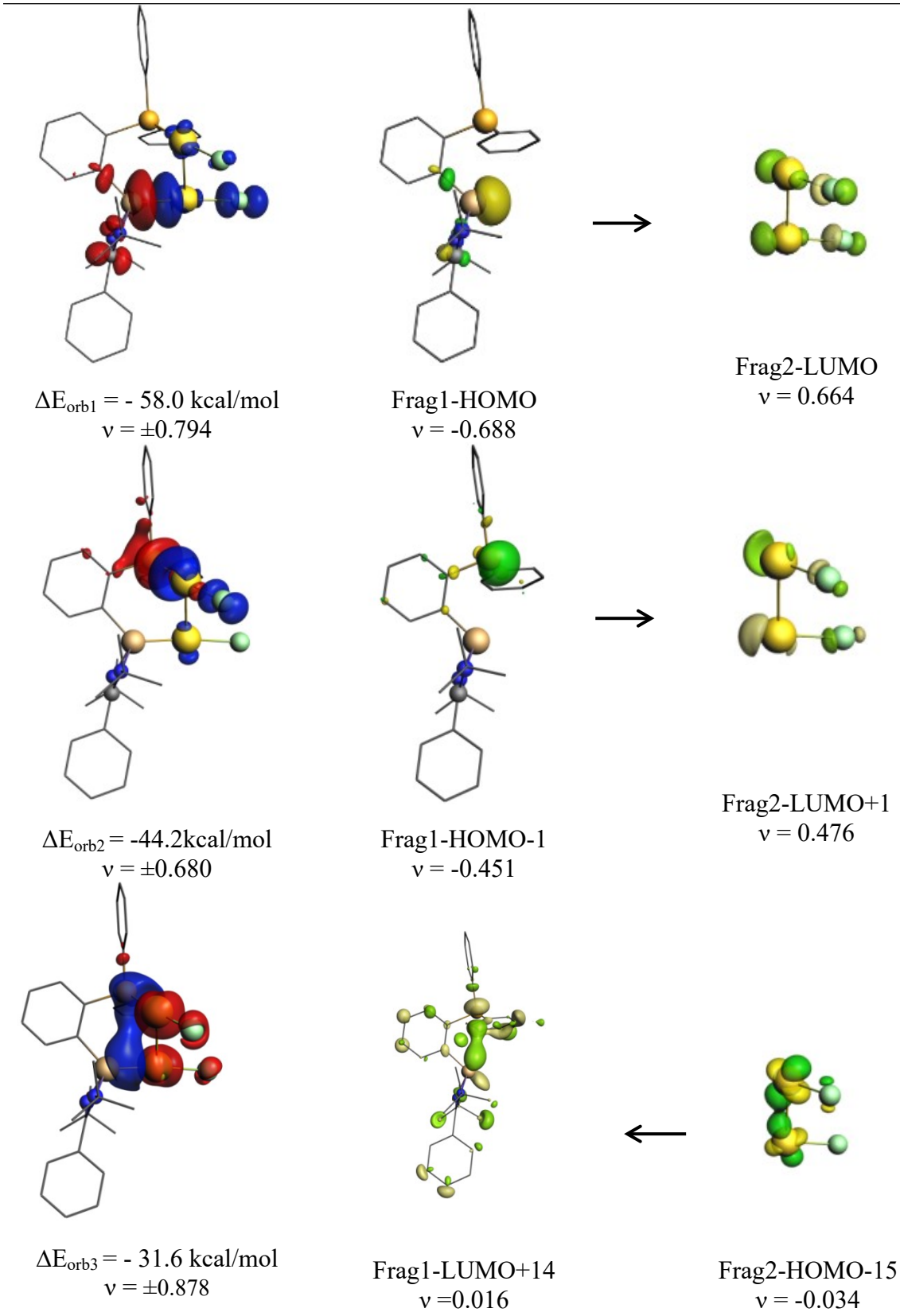

Figure S16. Shape of the most important interacting MOs of the two fragments **1** and 2AuCl(S) fragments in **2**, plot of deformation densities Δρ of the pairwise orbital interactions and the associated interaction energies (ΔE_{orb}) between fragments. The direction of the charge flow is red to blue.

Table S5. Topological parameters of selected bonds in compound **2**.[a]

Bond A1-A2	ρ(rBCP)[e Å^{-3}]	$\nabla^2\rho$(rBCP)[e Å^{-5}]	ε(BCP)	d_{BP}[Å]	d_{BCP-A1}[Å]	d_{BCP-A2}[Å]
Au1-Au2	0.030076	0.073245	0.076550	3.039	1.516	1.523
Au1-P	0.123301	0.050270	0.005793	2.249	0.850	1.399
Au1-Cl	0.098092	0.213192	0.033206	2.318	1.161	1.157

[a] d_{BP}: Bond path length, $d_{BCP-A1/2}$: distance of BCP to atom A1/2, ρ(rBCP): electron density at BCP, $\nabla^2\rho$(rBCP): Laplacian values at BCP, ε(BCP): ellipticity at BCP.

Table S6. EDA-NOCV results of complex 2PR-2AuCl by using interacting fragments 2PR and 2AuCl in their singlet (S) , doubled(D) states at P86+(D3BJ)/TZ2P level of theory. Energy values are given in kcal/mol.

Fragments	**2PR(S)+ 2AuCl(S)**	**2PR$^+$(D)+ 2AuCl$^-$(D)**	**2PR^{2+}(S)+ 2AuCl^{2-}(S)**	**2PR$^-$(D)+ 2AuCl$^+$(D)**	**2PR^{2-}(S)+ 2AuCl^{2-}(S)**
ΔE_{int}	-144.6	-222.8	-657.3	-385.5	-880.8
ΔE_{Pauli}	390.2	509.1	711.7	408.0	458.3
ΔE_{elstat}[a]	-345.2(64.6%)	-409.6(56.0%)	-706.9(51.6%)	-435.6(54.9%)	-633.7(47.3%)
ΔE_{disp}[a]	-31.0(5.8%)	-31.0(4.2%)	-31.0(2.2%)	-31.0(3.9%)	-31.0(2.3%)
ΔE_{orb}[a]	-158.5(29.6%)	-291.3(39.8%)	-631.0(46.1%)	-326.9(41.2%)	-674.4(50.4%)
ΔE_{orb1}[b]	-89.1(56.2%)				
ΔE_{orb2}[b]	-51.8(32.7%)				
$\Delta E_{orb(rest)}$[b]	-17.6(11.1%)				

[a]The values in parentheses give the percentage contribution to the total attractive interactions $\Delta E_{elstat} + \Delta E_{orb} + \Delta E_{disp.}$

[b]The values in parentheses give the percentage contribution to the total orbital interactions ΔE_{orb}.

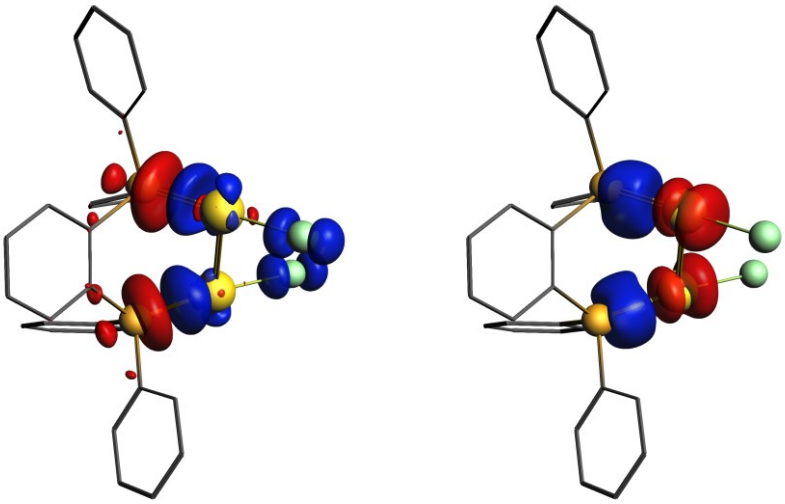

Δρ1
ΔE_{orb1}= -89.1
ν_1 = ±1.348

Δρ2
ΔE_{orb2}= -51.8
ν_2 = ±1.396

Figure S17. Plot of deformation densities (Δρ) of the pairwise orbital interactions in 2PR-2AuCl between the interacting 2PR and 2AuCl fragments, with the associated interaction energies (ΔEorb) in kcal/mol. The charge eigenvalues (ν) provide an estimate of the relative size of the charge migration. Direction of charge flow is from red to blue.

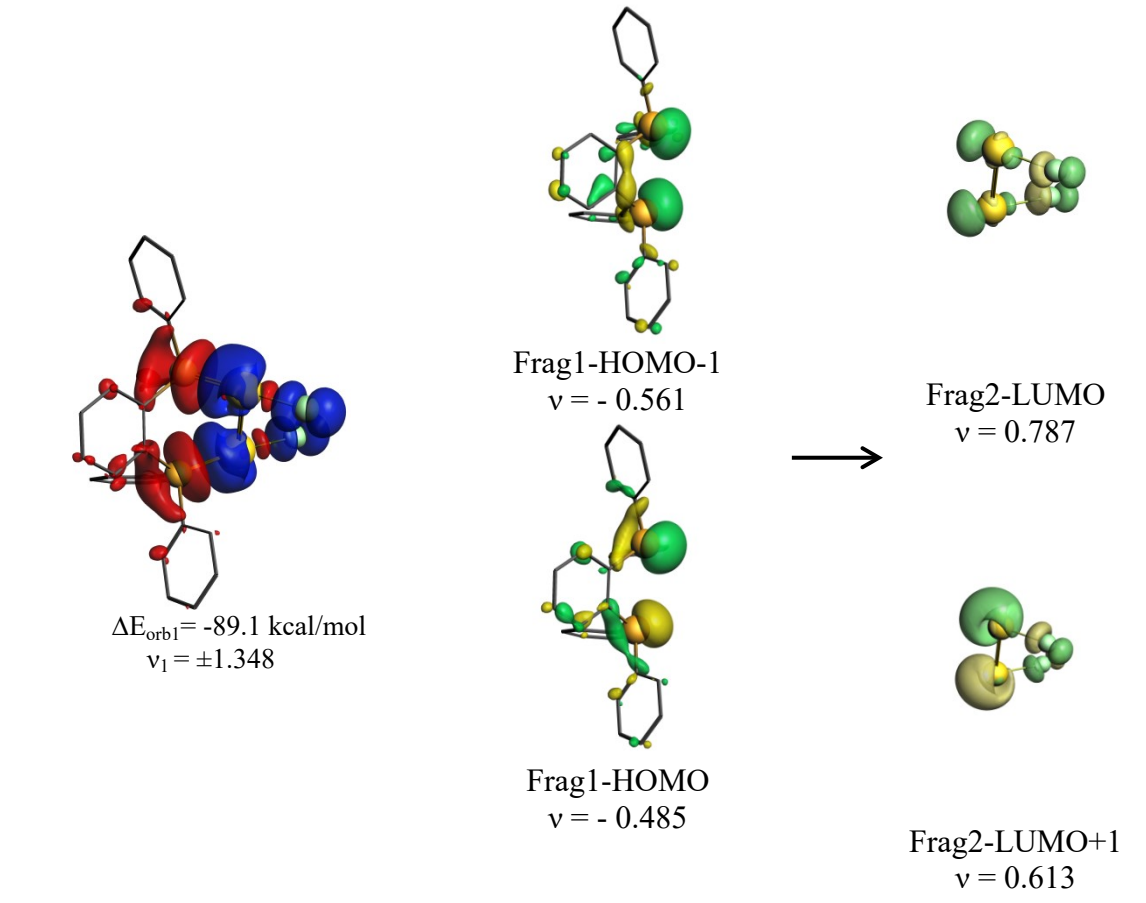

Figure S18. Shape of the most important interacting MOs of the two fragments 2PR(S) and 2AuCl(S) fragments in 2PR-2AuCl, plot of deformation densities Δρ of the pairwise orbital interactions and the associated interaction energies (ΔE_{orb}) between fragments. The direction of the charge flow is red to blue.

References

1. Bruker AXS Inc., in *Bruker Apex CCD, SAINT v8.40A* (Ed.: Bruker AXS Inst. Inc.), WI, USA, Madison, 2019.
2. L. Krause, R. Herbst-Irmer, G. M. Sheldrick, and D. Stalke, J. Appl. Crystallogr. 2015, **48**, 3-10.
3. M. Sevvana, M. Ruf, I. Usón, G. M. Sheldrick, and R. Herbst-Irmer, Acta Crystallogr., 2019, **D75**, 1040-1050.
4. G. M. Sheldrick, *Acta Crystallogr*. 2015, **A71**, 3-8.
5. G. M. Sheldrick, *Acta Crystallogr*. 2015, **C71**, 3-8.
6. C. B. Hübschle, G. M. Sheldrick, and B. Dittrich, *J. Appl. Crystallogr*. 2011, 44, 1281-1284.
7. M. J. Frisch, G. W. T., H. B. Schlegel, G. E. Scuseria, M. A. Robb, J. R. C., G. Scalmani,V. Barone, G. A. Petersson, H. N., X. Li, M. Caricato, A. V. Marenich, J. Bloino, B. G. J., R. Gomperts, B. Mennucci, H. P. Hratchian, J. V. Ortiz, A. F. I., J. L. Sonnenberg, D. Williams-Young, F. Ding, F. L., F. Egidi, J. Goings, B. Peng, A. Petrone, T. Henderson, D. R., V. G. Zakrzewski, J. Gao, N. Rega, G. Zheng, W. L., M. Hada, M. Ehara, K. Toyota, R. Fukuda, J. Hasegawa, M. I., T. Nakajima, Y. Honda, O. Kitao, H. Nakai, T. Vreven, K. T., J. A. Montgomery, Jr., J. E. Peralta, F. Ogliaro, M. J. B., J. J. Heyd, E. N. Brothers, K. N. Kudin, V. N. Staroverov, T. A. K., R. Kobayashi, J. Normand, K. Raghavachari, A. P. R., J. C. Burant, S. S. Iyengar, J. Tomasi, M. C., J. M. Millam, M. Klene, C. Adamo, R. Cammi, J. W. Ochterski, R. L. M., K. Morokuma, O. Farkas, J. B. Foresman and a. D. J. F., Gaussian, Inc., Wallingford CT, 2016., Gaussian 16, Revision A. 03.
8. (a) A. D. Becke, *Phys. Rev. A* 1988, **38**, 3098–3100; (b) J. P. Perdew, *Physical Review B* 1986, **33**, 8822–8824.
9. F. Weigend and R. Ahlrichs, *Physical Chemistry Chemical Physics* 2005, **7**, 3297–3305.
10. S. Grimme, J. Antony, S. Ehrlich and H. Krieg, *The Journal of Chemical Physics* 2010, **132** .
11. A. V. Marenich, C. J. Cramer and D. G. Truhlar, *J. Phys. Chemistry B* 2009, **113** , 6378–6396.
12. (a) E. R. Johnson, S. Keinan, P. Mori-Sánchez, J. Contreras-García, A. J. Cohen and W. Yang, *J. Am. Chem. Soc.* 2010, **132**, 6498–6506; (b) T. Lu, F. Chen, *J. Computational Chem.* 2012, **33**, 580–592.
13. R. F. W. Bader, *A Quantum Theory.* 1990.
14. T. A. K. AIMAll (Version 17.11.14), T. G. S., Overland Park KS, USA, 2017, TK Gristmill Software. 2017.
15. C. Y. Legault, CYLview20, Université de Sherbrooke 2020.
16. T. Ziegler and A. Rauk, *Theoretica chimica acta* 1977, **46**, 1–10.
17. (a) M. Mitoraj and A. Michalak, *Organometallics* 2007, **26**, 6576-6580; (b) M. Mitoraj and A. Michalak, *J. Mol. Model.* 2008, **14**, 681–687.
18. G. te Velde, F. M. Bickelhaupt, E. J. Baerends, C. Fonseca Guerra, S. J. A. van Gisbergen, J. G. Snijders and T. Ziegler, *J. Comput. Chem.* 2001, **22**, 931–967.

19. F. M. Bickelhaupt, N. M. M. Nibbering, E. M. Van Wezenbeek and E. J. Baerends, *J. Phys. Chem.* 1992, **96**, 4864–4873.
20. (a) F. M. Bickelhaupt and G. Frenking, (Eds.: G. Frenking, S. S. S., 2014, 121–157; (b) A. Krapp, F. M. Bickelhaupt and G. Frenking, *Chem. Eur. J.* 2006, **12**, 9196–9216; (c) L. Zhao, S. Pan, N. Holzmann, P. Schwerdtfeger and G. Frenking, *Chem. Rev.* 2019, **119**, 8781–8845; (d) L. Zhao, W. H. E. Schwarz and G. Frenking, *Nature Reviews Chemistry* 2019, **3**, 35–47.